Minimum thickness of liquid film for the validity of water hammer theory

Kazumichi Kobayashi,[1, a)] Jotaro Akazawa,[1] Kotaro Ohashi,[1] Mikihiro Muramatsu,[1] Takuro Nagakawa,[1] Hiroyuki Fujii,[1] and Masao Watanabe[1]
Division of Mechanical and Space Engineering, Faculty of Engineering, Hokkaido University, Sapporo, 060-8628 Japan

(Dated: 7 August 2025)

Systems that clean by high-speed nanodroplet injection have recently been developed; however, elucidating the cleaning mechanism underlying nanodroplet impact is urgently required. In this study, numerical simulations of the high-speed impact phenomenon of two liquid films were performed using the Enskog–Vlasov direct simulation Monte Carlo method. We determine the minimum liquid film thickness for which the water hammer theory is applicable to the maximum pressure generated during liquid film impact. The simulation results show that the water hammer pressure was generated when the liquid film thickness exceeded the compression wavefront thickness generated by the liquid film impact, which is more than ten times the molecular diameter.

Droplet impact is an important physical phenomenon in various industrial fields[1–3]. Cleaning techniques that use high-speed nanodroplet impacts have recently been developed[4–6]. For example, Xiao et al. reported a mist spray (composed of nanodroplets) accelerated by a nozzle and ejected at supersonic speeds[5]. Furthermore, these nanodroplets kill bacteria by impacting them at high speeds[6]. Cleaning technology leveraging nanodroplet impact will continue to improve; however, its cleaning mechanism has not yet been elucidated. Proposed cleaning mechanisms have been attributed to various factors, including chemical and physical effects; however, this study focused on the physical effects of impact pressure.

When a sufficiently thick liquid impacts, the pressure at the point of impact is the well-known water hammer pressure[7–9]. The impact pressure p_{wh} can be expressed by the following equation:

$$p_{\mathrm{wh}} = \rho S V, \tag{1}$$

where ρ denotes the fluid density, V is the impact speed, and S is the propagation speed of the compression wave generated at the impact point. It has been shown that this water hammer pressure is also valid for the impact of liquid droplets with curved interfaces, and not just for flat liquid surfaces[9]. The water hammer theory is a well-known phenomenon historically studied using fluid dynamics. In recent studies, much attention has been focused on industrial applications, such as the effects of channel geometry and material properties on the generation of impact pressure, and the elucidation of complex pressure fields created by compressible flow fields and water hammer pressure[10,11]. In cases where the flow field becomes small, it is well known, particularly in gas flows, that fluid dynamics breaks down in the high Knudsen number regime. However, for liquids, it remains unclear to what extent internal flow fields continue to follow the equations of fluid dynamics as the system size decreases. In particular, whether the water hammer theory remains valid within small liquid volumes has not yet been fully clarified. In other words, it is still uncertain whether Eq. (1) in this study is applicable to nanoscale droplet impacts.

Many studies have been conducted using molecular dynamics to simulate the impact of nanodroplets (for example, Refs. 12–15). However, most of these studies have focused on the spreading and rebounding of droplets. In this study, we focused on the high-speed impact of two liquid films, as shown in Fig. 1(a), where two liquid films of thickness δ moving at the same speed V collide head-on; high pressure is generated at the point of impact. As shown in Fig. 1(b), compression waves propagate from the point of impact. By measuring the difference in the wavefront positions at times τ_1 and τ_2, the propagation speed S can be calculated. The main objective is to investigate the lower limit of the liquid film thickness to which Eq. (1) can be applied. If we can determine the lower limit of the liquid film thickness for which the theory of fluid dynamics (water hammer theory) applies, then we no longer need to perform a molecular-scale analysis of droplets with diameters larger than that thickness. Furthermore, in the

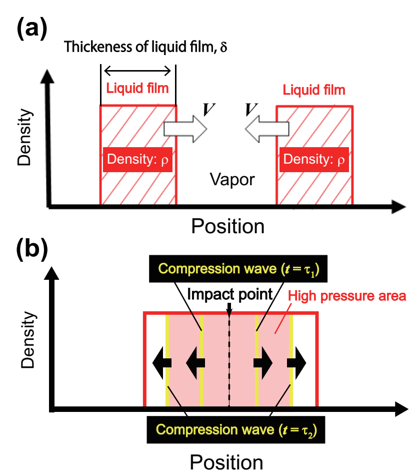

FIG. 1. Schematic representation of the impact between two liquid films: (a) before impact; (b) after impact.

a)Electronic mail: kobakazu@eng.hokudai.ac.jp

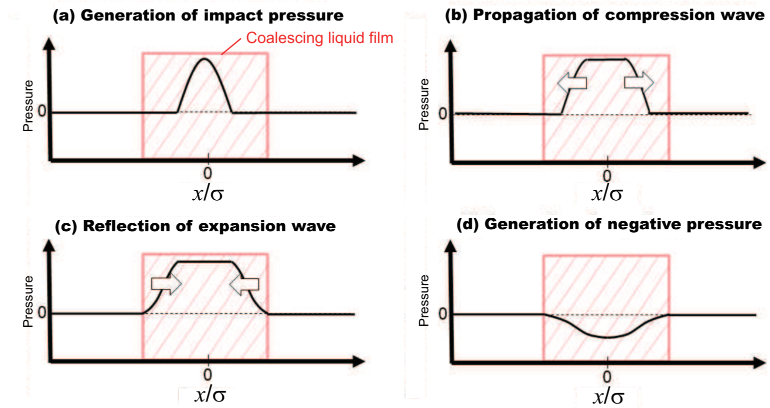

FIG. 2. Schematics of the impact problem of the two liquid films and the generation and propagation of the pressure wave inside the liquid film. The solid red line shows the liquid phase and the solid black line shows the pressure. The horizontal axis is the nondimensional position x/σ, where σ is the molecular diameter.

previous study[6], the maximum pressure required to inactivate viruses has been discussed using the water hammer theory. Through the present study, it will become possible to conduct a more detailed investigation of this value, especially for nanoscale droplets. Thus, it is necessary to accurately determine this lower limit.

We modeled the problem described above as a one-dimensional spatial problem and analyzed it using the mean-field kinetic theory (Enskog–Vlasov equation). The Enskog–Vlasov equation extends the Boltzmann equation and describes gases and high-density fluids (liquids). The numerical method used to solve the Enskog–Vlasov equation is the Enskog–Vlasov DSMC method (EVDSMC method) proposed by Frezzotti[16–18]. The detailed procedure for the EVDSMC method or an overview is presented by Refs. 19 and 20. This particle simulation method can use many sample molecules in the analysis. Because this analysis approach uses many more particles than do molecular dynamics analyses, we can perform an unsteady problem analysis with fewer statistical errors. The run time is approximately 100 times less than that for the molecular dynamics simulation when the problem is spatially one–dimensional[21]. We report the results of a detailed study to assess whether the maximum impact pressure

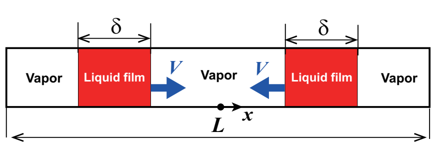

FIG. 3. Schematic of numerical simulation system used to assess the impact of two liquid films.

becomes the water hammer pressure by changing the thickness of the liquid film and the impact speed.

The physical phenomena of the generation and propagation of pressure waves inside the liquid film after impact between the two liquids are shown in Fig. 2. The horizontal axis represents the nondimensional position x/σ, where σ is the molecular diameter. The solid red line represents the liquid phase, and the solid black line represents the pressure profile.

As shown in Fig. 2(a), when the two liquids collide, high pressure is generated at the point of impact. If the water hammer theory is used, Eq. (1) can be used to express the maximum pressure. Subsequently, the compression waves maintaining the maximum pressure behind the wavefront propagate through the liquid film and toward the vapor–liquid interfaces (Fig. 2(b)). Then, the compression wave is reflected at the vapor–liquid interface. However, owing to the large difference in acoustic impedance, it is reflected as an expansion wave (Fig. 2(c)). This expansion wave converges at the point of impact of the liquid film, forming a high-negative pressure (Fig. 2(d)).

Furthermore, this expansion wave propagates to the vapor–liquid interface, is reflected at the interface, and then becomes a compression wave that propagates to the center of the liquid film and converges. Thus, at the moment of impact of the liquid film, the pressure field inside the liquid film alternates between positive and negative.

Because both liquid films have an impact speed V, the relative impact speed of the two liquid films is $2V$. However, the maximum pressure is halved when liquids with the same acoustic impedance impact each other[22]. In this simulation system, the maximum pressure at which the water hammer pressure is valid can be expressed using V in Eq. (1).

As shown in Fig. 3, we simulated a one-dimensional problem. The two liquid films were placed at the same distance

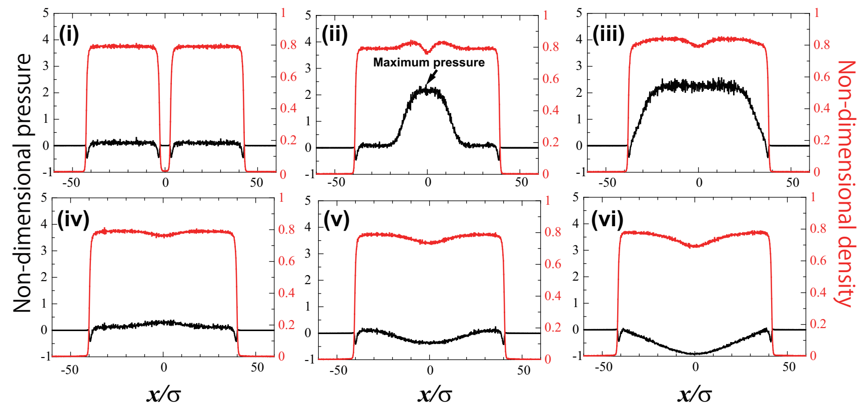

FIG. 4. Snapshots of time variation in the density and pressure distributions for the impact of two liquid films: (i) t/t_0=0; (ii) t/t_0=12.5; (iii) t/t_0=16.5; (iv) t/t_0=26.5; (v) t/t_0=28.5; and (vi) t/t_0=32.5. The liquid film thickness is 39.4σ, and the impact speed is $V/a_0 = 0.4$.

from the center of the system. The size of the simulation system L was set to 100σ, 120σ, or 250σ. The size depended on the thickness of the liquid film. In addition, the system was assigned periodic boundary conditions at both ends.

First, we performed a simulation of a vapor–liquid equilibrium system. For the initial equilibrium state, we set the initial liquid film thicknesses to 10σ, 15σ, 20σ, 30σ, 40σ, 50σ, and 100σ. After the system reached equilibrium, the liquid film thicknesses were $\delta = 8.0\sigma$, 12.0σ, 15.8σ, 23.8σ, 31.4σ, 39.4σ, and 95.8σ, respectively. The liquid film thickness after equilibrium was defined based on the positions at which the density at the liquid film interface was half that of the liquid. We confirmed that the liquid and vapor densities at stationary equilibrium were the same as those in previous studies[23,24]. The initial temperature was set to $0.6T_c$, where T_c is the critical temperature. The temperature of $0.6T_c$ corresponds to conditions near the triple point of monoatomic molecules such as argon, thereby simulating a vapor-liquid two-phase system in the low-temperature regime[17,23].

In this study, a one-dimensional system is considered, allowing the compression waves generated by the collision to be treated as planar waves. This simplifies the evaluation, as opposed to the spherical waves generated in three-dimensional droplet impacts. Furthermore, by considering the impact of two liquid films, the need to account for the finite acoustic impedance of a wall is removed, making it easier to discuss the applicability of the water hammer theory.

We subsequently assigned the same speed to the two liquid films that were facing each other, which then collided head on. The liquid film speed V was varied with respect to the speed of sound of the vapor $a_0 = \sqrt{5k_B(0.6T_c)/(3m)}$, where k_B is the Boltzmann constant and m is the mass of a molecule. In this study, monoatomic molecules modeled with the Sutherland potential are used, and thus the specific heat ratio of the monoatomic gas is 5/3. The liquid film speed was varied according to $V/a_0 = \mathrm{Ma} = 0.4, 0.8, 1.0$, where Ma denotes the Mach number. The macroscopic quantities of fluid, as well as the number density n and pressure p obtained from the simulation were nondimensionalized; they are as follows: n/n_c, $p/(n_c k_B T_c)$, and $V/\sqrt{2k_B(0.6T_c)/m}$, where n_c is the critical number density. Time t was nondimensionalized by $t_0 = \sigma/\sqrt{2k_B(0.6T_c)/m}$. In general, the most probable speed ($\sqrt{2k_B T/m}$) is adopted as the representative velocity in kinetic simulations, and the same approach is employed in this study[25]. In the Enskog–Vlasov DSMC analysis, the cell size was set to $\Delta x/\sigma = 0.2$ and the time increment was set to $\Delta t/t_0 = 0.0005$. The number of particles used in the analysis ranged from 1,250,000 to 6,250,000.

Figure 4 shows the results of the simulated liquid–film impact, where the solid red line denotes density and the solid black line denotes pressure. The results shown are for a liquid film thickness of 39.4σ and an impact speed of $V/a_0 = 0.4$. The result immediately before the impact of the two liquid films is presented in Fig. 4(i). After the impact, high pressure was generated at the point (Fig. 4(ii)). Compression waves were generated in this high-pressure area, and the waves propagated toward both ends of the vapor–liquid interface (Fig. 4(iii)). The compression waves were then reflected at the interface; the expansion wave was reflected due to the difference in acoustic impedance, and the waves converged at the center of the liquid film (Figs. 4(iv)–(vi)). Thus, the phenomenon described in Fig. 2 was confirmed by simulation.

The time variation in the pressure at the center of the liquid film (the liquid film impact point) is shown for the impact speed of $V/a_0 = 0.4$ in Fig. 5. Figure 5(a) shows the case in which the liquid film thickness δ is 8.0σ, and Fig. 5(b) shows the case in which the liquid film thickness is 39.4σ. The results show that the positive and negative pressures alternate at the point of impact. The first pressure peak was the maximum pressure, which decreased over time. From these figures, it can be seen that the pressure inside the liquid film

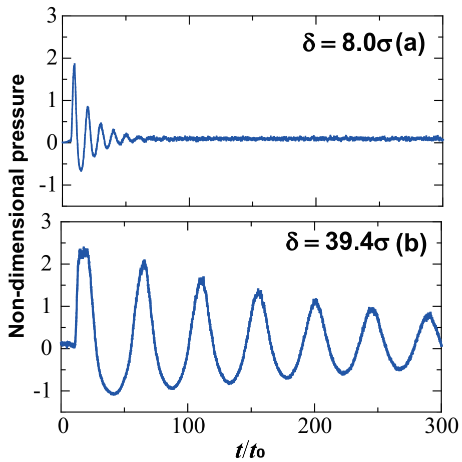

FIG. 5. Time variation of pressure at the impact point of thin and thick liquid films at the impact speed is $V/a_0 = 0.4$: (a) $\delta = 8.0\sigma$; and (b) $\delta = 39.4\sigma$.

alternates between positive and negative pressures. A comparison of Figs. 5(a) and 5(b) shows that the decay rates of the pressure peak increase as the liquid film becomes thinner.

Figure 6(a) shows the calculated wave propagation speed of the compression wave, S. The horizontal and vertical axes represent the impact speed and propagation speed of the compression wave, respectively. These results show that the propagation speed increases slightly as the impact speed increases.

Figure 6(b) shows the relationship between the maximum impact pressure and the liquid film thickness. Red, blue, and green indicate the results for the impact speeds of $0.4a_0$, $0.8a_0$, and $1.0a_0$. The dashed line shows the plot of Eq. (1), where the density is in an equilibrium state before the impact.

The results plotted in this figure show that the greater the impact speed, the higher the maximum pressure. Furthermore, when the liquid film is sufficiently thick, the maximum pressure is a constant value at all impact speeds. These findings are consistent with the results obtained using Eq. (1). However, the maximum pressure decreases when the liquid film is thinner.

Figure 6(c) shows the results of Fig. 6(b) divided by the water hammer pressure (expressed by Eq. (1)) at all the impact speeds. These results show that the relationship between each impact speed and the liquid film thickness is almost the same. When the liquid film thickness is approximately 15σ or less, it can be observed that the results related to Eq. (1) do not match.

We investigated the reasons why Eq. (1) does not hold when the liquid film becomes thin. Figure 7 shows the compression wavefront thickness for various impact speeds under maximum pressure immediately after impact (see Fig. 4(ii)). For all results, the liquid film thickness is $\delta = 39.4\sigma$, which is

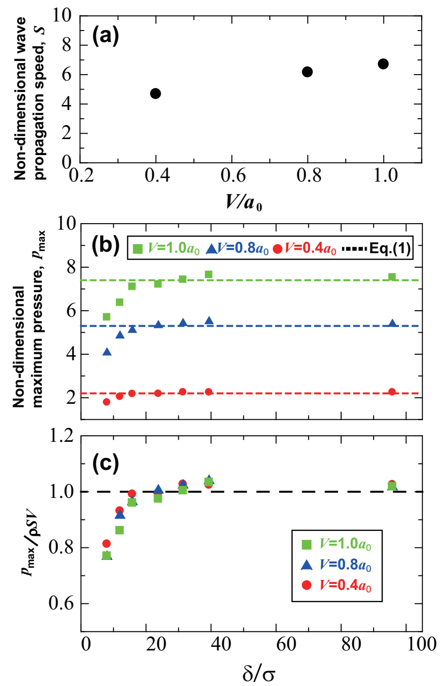

FIG. 6. Relationship between the maximum pressure and liquid film thickness: (a) wave propagation speed, S, vs. impact speed, V; (b) maximum pressure, $p_{\max}$, vs. liquid film thickness, δ; (c) $p_{\max}/\rho SV$ vs. liquid film thickness.

sufficient to establish water hammer pressure (see Fig. 6(b) or (c)). The vertical axis is normalized by the value of the maximum pressure, and the horizontal axis, x, is offset such that half of the pressure value is $x_{\text{off}} = 0$ on the horizontal axis.

From this figure, it can be interpreted that the pressure wavefront is a region in which the pressure changes continuously. As the impact speed increases, the wavefront appears to become slightly thinner; however, its thickness can be considered to be more than ten times the diameter of the molecule. This result indicates that if the liquid film is sufficiently thicker than the wavefront, then the maximum pressure is given by Eq. (1). When the thickness of the liquid film is almost the same as (or less than) the thickness of the wavefront, the compression waves generated by the impact do not form normally, and the maximum pressure becomes low. For the same reason, the rate of pressure decay increases as the liquid film becomes thinner, as shown in Fig. 5. These results indicate that if the molecular diameter is about 0.35 nm (argon molecule), the water hammer pressure can be satisfied with an approximate liquid film thickness of about 5.3 nm ($=15\times\sigma$).

In the present study, the gas phase between the liquid films consists solely of vapor. As a result, the vapor between the

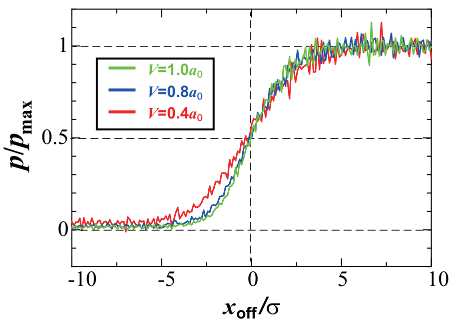

FIG. 7. Pressure wavefront shapes generated at various impact speeds. The pressure is nondimensionalized by the maximum pressure. The liquid film thickness is 39.4σ

approaching liquid films rapidly condenses at the interfaces, allowing the films to move at nearly constant velocity and collide without significant deceleration. In our simulations, the initial distance between the liquid films ranges approximately from 10σ to 40σ, depending on the film thickness. The difference between the initial and pre-impact velocities is found to be at most around 2.9%, indicating that the difference in initial distance has minimal impact on this simulation.

At the temperature used in this study ($0.6T_c$), the transition layer thickness, determined using the 10–90 thickness method, is approximately 3σ (see Ref. Kon, Kobayashi, and Watanabe [23]). While our results show that the water hammer theory becomes invalid when the liquid film thickness is thinner than the wavefront thickness, the interfacial transition layer remains thin in comparison and is therefore expected to have negligible influence on the results. Nevertheless, the effect is expected to become increasingly significant at higher temperatures. This is due to the fact that the interfacial transition layer tends to become thicker as the temperature increases.

In this study, fast impacts with Ma numbers greater than 0.4 were examined, but studies with slower impact speeds are planned for the future. This is because, in the case of slow speed impacts, the maximum pressure becomes lower and the wavefront thickness becomes thicker, requiring a more precise analysis than the one conducted in this study. Furthermore, in the vicinity of the vapor–liquid interface, a potential field is generated by the molecules constituting the liquid. When the liquid film (or droplet) speed is slow, the influence of this potential field becomes significant, potentially altering the impact speed of the film.

It is reiterated that the central conclusion of this study is that the water hammer theory is applicable when the liquid film thickness exceeds that of the compression wave generated by the impact.

ACKNOWLEDGMENTS

This work was supported by JSPS KAKENHI (Grant No. JP24K00797 and No. JP25H00405), JST, and PRESTO (Grant No. JPMJPR21O3, Japan).

CONFLICT OF INTEREST

The authors have no conflicts to disclose.

DATA AVAILABILITY

Data supporting the findings of this study are available from the corresponding author upon request.

REFERENCES

[1] W. Zhang, C. A. Dorao, and M. Fernandino, "Relaxation phase during droplet impact on superhydrophobic surfaces with high contact angle hysteresis," Appl. Phys. Lett. **123**, 111602 (2023).
[2] J. Luo, F. Chu, J. Zhang, and D. Wen, "Re-spreading behavior of droplet impact on superhydrophobic surfaces at low weber numbers," Appl. Phys. Lett. **123**, 061604 (2023).
[3] A. Aihara, M. Tanaka, and N. Fujisawa, "Influence of surface curvature on the impact force of water droplet," J. Appl. Phys. **136**, 114701 (2024).
[4] S. Uehara, T. Nakajima, S. Moriya, S. Maruyama, and T. Sato, "Removal mechanism of artificial dental plaque by impact of micro-droplets," ECS J. Solid State Sci. Tech. **8**, N20 (2019).
[5] Y. Xiao, S. Liu, T. Nakajima, and T. Sato, "Characteristics of high-speed mist generated by condensation of water vapor in pressurized air," Int. J. Plasma Env. Sci. Tech. **16**, e03003 (2022).
[6] Y. Tamura, M. Kawamura, T. Sato, T. Nakajima, S. Liu, T. Sato, and S. Fujimura, "Impact of high-speed nanodroplets on various pathogenic bacterial cell walls," J. Bacteriol. **206**, e00139–24 (2024).
[7] M. S. Ghidaoui, M. Zhao, D. A. McInnis, and D. H. Axworthy, "A review of water hammer theory and practice," Appl. Mech. Rev. **58**, 49–76 (2005).
[8] T. Leighton, *The acoustic bubble* (Academic press, 2012).
[9] Y. Tatekura, M. Watanabe, K. Kobayashi, and T. Sanada, "Pressure generated at the instant of impact between a liquid droplet and solid surface," R. Soc. Open Sci. **5**, 181101 (2018).
[10] M. Kandil, T. A. El-Sayed, and A. Kamal, "Unveiling the impact of pipe materials on water hammer in pressure pipelines: An experimental and numerical study," Sci. Rep. **14**, 30599 (2024).
[11] G. Tretola and K. Vogiatzaki, "Unveiling the dynamics of ultra high velocity droplet impact on solid surfaces," Sci. Rep. **12**, 7416 (2022).
[12] J. Koplik and R. Zhang, "Nanodrop impact on solid surfaces," Phys. Fluids **25**, 022003 (2013).
[13] K. Kobayashi, K. Konno, H. Yaguchi, H. Fujii, T. Sanada, and M. Watanabe, "Early stage of nanodroplet impact on solid wall," Phys. Fluids **28**, 032002 (2016).
[14] N.-N. Han, S.-W. Wang, B.-M. Sun, and X. He, "Nanodroplet impacts on hydrophobic/superhydrophobic surfaces with point textures," J. Appl. Phys. **132**, 205302 (2022).
[15] Y. Tian, M. Ma, Z. Chen, K. Cui, J. Du, C. Yu, S. Wang, and X. He, "Collision of nanoscale water droplets: A molecular dynamics study," Phys. Fluids **37** (2025).
[16] A. Frezzotti, "A particle scheme for the numerical solution of the Enskog equation," Phys. Fluids **9**, 1329–1335 (1997).
[17] A. Frezzotti, L. Gibelli, and S. Lorenzani, "Mean field kinetic theory description of evaporation of a fluid into vacuum," Phys. Fluids **17**, 012102 (2005).

[18] A. Frezzotti, L. Gibelli, D. A. Lockerby, and J. E. Sprittles, "Mean-field kinetic theory approach to evaporation of a binary liquid into vacuum," Phys. Rev. Fluids **3**, 054001 (2018).
[19] A. Frezzotti, P. Barbante, and L. Gibelli, "Direct simulation Monte Carlo applications to liquid-vapor flows," Phys. Fluids **31**, 062103 (2019).
[20] S. Busuioc, L. Gibelli, D. A. Lockerby, and J. E. Sprittles, "Velocity distribution function of spontaneously evaporating atoms," Phys. Rev. Fluids **5**, 103401 (2020).
[21] A. Frezzotti and P. Barbante, "Kinetic theory aspects of non-equilibrium liquid-vapor flows," Mech. Eng. Reviews **4**, 16–00540–16–00540 (2017).
[22] E. Johnsen and T. Colonius, "Numerical simulations of non-spherical bubble collapse," J. Fluid Mech. **629**, 231–262 (2009).
[23] M. Kon, K. Kobayashi, and M. Watanabe, "Method of determining kinetic boundary conditions in net evaporation/condensation," Phys. Fluids **26**, 072003 (2014).
[24] K. Ohashi, K. Kobayashi, H. Fujii, and M. Watanabe, "Mean-field kinetic theory analysis of vapor flow between evaporating and condensing interfaces in the presence of non-condensable gas molecules," Phys. Fluids **33** (2021).
[25] G. A. Bird, *Molecular gas dynamics and the direct simulation of gas flows* (Clarendon press Oxford, 1994).